ELSEVIER

Nuclear Instruments and Methods in Physics Research A 432 (1999) 48–65

NUCLEAR INSTRUMENTS & METHODS IN PHYSICS RESEARCH Section A

www.elsevier.nl/locate/nima

A systematic measurement of energy resolution and e/π ratio of a lead/plastic-scintillator sampling calorimeter

T. Suzuki[a], Y. Fujii[b,*], K. Hara[a], T. Ishizaki[a], F. Kajino[d], N. Kanaya[c], J. Kanzaki[b], K. Kawagoe[c], S. Kim[a], T. Matsui[b], A. Miyajima[e], A. Nakagawa[a], S. Nakazawa[c,1], M. Nozaki[c], T. Ota[a], K. Sendai[b], Y. Sugimoto[b], Y. Sugimoto[c], H. Takayama[a,2], H. Takeda[c], T. Takeshita[e], S. Tanaka[c,3], A. Tanaka[d,4], T. Toeda[e,5], Y. Yamada[d]

[a]*Institute of Physics, University of Tsukuba, Tsukuba, Ibaraki 305-8571, Japan*
[b]*Institute of Particle and Nuclear Studies, High Energy Accelerator Research Organization, Tsukuba, Ibaraki 305-0801, Japan*
[c]*Department of Physics, Kobe University, Kobe, Hyogo 657-8501, Japan*
[d]*Department of Physics, Konan University, Kobe, Hyogo 658-8501, Japan*
[e]*Department of Physics, Shinshu University, Matsumoto, Nagano 390-8621, Japan*

Received 5 January 1999

Abstract

The energy resolution and the e/π ratio of a lead/plastic-scintillator sampling calorimeter were measured for various volume ratios of the lead thickness to the scintillator thickness. For this purpose, a hanging-file-type calorimeter module was constructed in which the thicknesses of the lead absorber and the plastic-scintillator plates were able to be altered very flexibly. The thicknesses of the lead and the scintillator plates can be changed by a 2 mm step form 4 to 16 mm and from 2 to 6 mm, respectively. We measured energy resolution for electrons and pions with the calorimeter module as a function of the thickness of a lead plate in the energy range 1–4 GeV. The best energy resolution for pions was obtained to be $33.6\%/\sqrt{E}$ with the configuration where the thicknesses of the lead and the scintillator plates were 4 and 2 mm, respectively. The e/π ratio was measured in the energy range 1–4 GeV. The compensation was found to be achieved for the lead thickness of 9.1 ± 0.3 mm in the case of 2 mm-thick scintillator.

PACS: 29.40.Mc; 29.40.Vj

Keywords: Calorimeter; Tile/fiber; Compensation; Linear collider

* Corresponding author. Tel.: + 81-298-64-5369; fax: 81-298-64-2580.
E-mail address: yoshiaki.fujii@kek.jp (Y. Fujii)
[1] Present address: FUJITSU LIMITED, Kawasaki, Kanagawa, Japan
[2] Present address: Department of Physics, Tohoku University, Sendai, Miyagi 980-8578, Japan
[3] Present address: Institute of Particle and Nuclear Studies, High Energy Accelerator Research Organization, Tsukuba, Ibaraki 305-0801, Japan
[4] Present address: Netwave Co. Ltd., Kyoto, 604-8112, Japan
[5] Present address: Department of Physics, Nagoya University, Nagoya, Aichi 464-8602, Japan

0168-9002/99/$ - see front matter
PII: S0168-9002(99)00394-0

1. Introduction

In the future linear collider experiments, a good hadron energy measurement is indispensable to have good sensitivities to new physics as well as to perform precise measurements of the Standard Model [1]. To achieve a good hadron energy resolution, compensation plays a crucial role in sampling calorimeters [2]. In general, the pulse height of calorimeter is different for electromagnetic (EM) showers and for hadron showers. The compensation is a condition that a calorimeter is made to have equal pulse height for EM showers and for hadron component in hadron showers; namely,

$$\mathrm{e/h} \equiv \frac{\text{pulse height for EM showers}}{\text{pulse height for hadron component in hadron showers}} = 1 \quad (1)$$

for the compensated calorimeters. This minimizes the degradation of hadron energy resolution due to fluctuation of the EM component in hadron shower development, and hence minimizes non-Gaussian behaviour and constant term of energy resolution and achieve good linearity for energy measurement. This condition can be achieved by adjusting the calorimeter configuration properly; what to use for active and absorber materials, and their thicknesses.

Experimentally e/π ratio is commonly used to estimate a degree of compensation. The e/π ratio is defined as

$$\mathrm{e/\pi} \equiv \frac{\text{pulse height for EM showers}}{\text{pulse height for charged pions}}. \quad (2)$$

Empirical relation between the e/h ratio and the e/π ratio is described in Ref. [3]. The result of some experiments about e/π ratio [4–6], and calculations of e/h ratio [2] indicate that a calorimeter consisting of lead and plastic scintillator with a volume ratio of about 4 : 1 may achieve compensation. However, the e/π ratio approaches 1.0 at higher energies regardless of compensation due to increase of π^0 component in the hadron shower. The results of the above experiments are $\mathrm{e/\pi} \sim 1.1$ for $E \leq 10\,\mathrm{GeV}$, and more systematic study is necessary to confirm the achievability of compensation.

As mentioned above, the e/h ratio, or the e/π ratio, is a function of the volume ratio of the

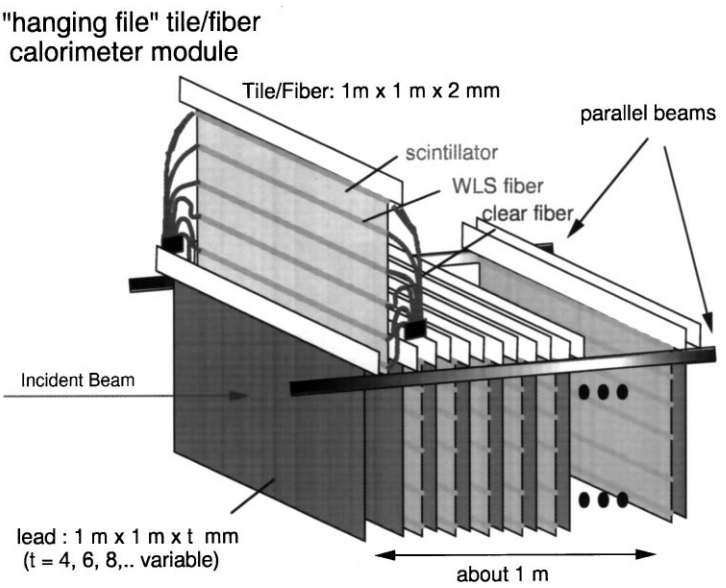

Fig. 1. Schematic view of the hanging-file type calorimeter module.

absorber and the active material [2]. However, it has not been measured systematically for the combination of lead and plastic scintillator. For this purpose, we constructed a hanging-file type calorimeter module and performed beam tests to measure the volume ratio dependence of the energy resolution and the e/π ratio.

In Section 2, we describe the optical characteristics of the plastic scintillator tile/fiber system used for the calorimeter module. The experimental setup is briefly described in Section 3. The analysis procedure is described in Section 4. The results are given in Section 5.

2. Calorimeter module

The calorimeter module consists of lead absorber and plastic scintillator plates of "hanging-file" configuration, where the absorber plates and scintillator plates are hung over a pair of parallel beams, as shown in Fig. 1. The thicknesses of the lead plates can be changed from 4 to 16 mm with a step of 2 mm. The thickness of the scintillator plates is fixed to 2 mm for measurements described in this paper.

Tile/fiber techniques are employed in order to easily alter the absorber thicknesses and optical readout system. The optical configuration of the tile/fiber system is shown in Fig. 2. A scintillator plate is 1×1 m, and 2 mm thick. Each scintillator plate has six straight grooves with a key hole shape with a groove distance of 20 cm. The four sides of the plates are painted white with TiO_2-based emulsion paint (Nippon Paint 'Odecoat'). The scintillator plates are covered in TiO_2-added white PET films. The fiber is made up of a 1 m long wavelength-shifter fiber (WLS fiber) spliced at the each end to a clear fiber by a heat-fusing method [11]. The diameter of the fibers is 1 mm. Kuraray SCSN38 and SCSN88 polystyrene-based scintillators and Y11 multiclad WLS fibers [7–10] are used.

In the beam tests, clear fibers from five successive scintillator layers are bundled to make a superlayer. Each side of the clear fiber bundle is connected to a phototube (HAMAMATSU H1949).

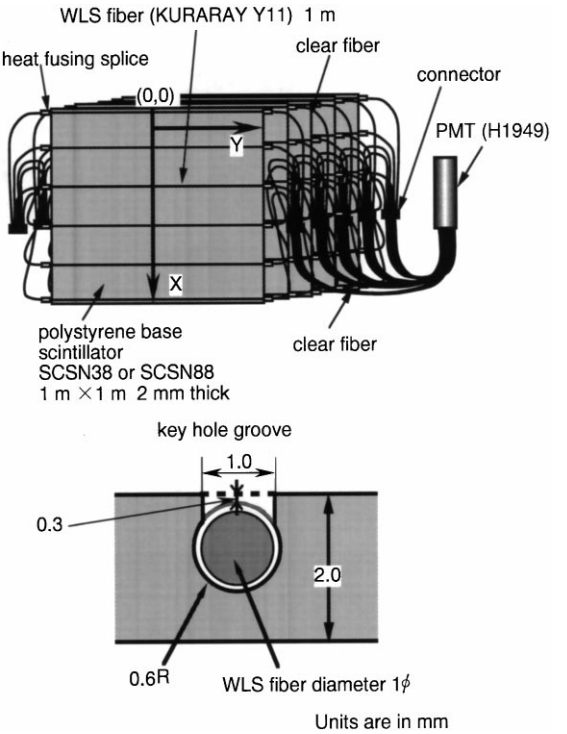

Fig. 2. Optical configuration of the tile/fiber system for the hanging-file type calorimeter module.

The light yield of the tile/fiber systems was measured at a test bench using penetrating β-rays from a ^{90}Sr source. Response mapping was carried out in both parallel and perpendicular directions to the WLS fibers using an automatic scanning system. In the direction perpendicular to the fibers, the light yield peaked at the points near the fibers as shown in Fig. 3. In the direction parallel to the fibers, the light yield was fairly flat except the points near the tile edge as shown in Fig. 4.

The distribution of the average light yield and non-uniformity in the direction perpendicular to the fibers (except the points near the fibers) are shown in Fig. 5. The mean light yield and its rms variation were 1.7 photoelectrons/mip (minimum ionizing particle) and 14.3%, respectively. Note that the variation did not include those of the PMTs and clear fibers used for the beam tests: we used the same system through the test bench measurements. The mean and rms variation of non-uniformity in a tile in the direction perpendicular

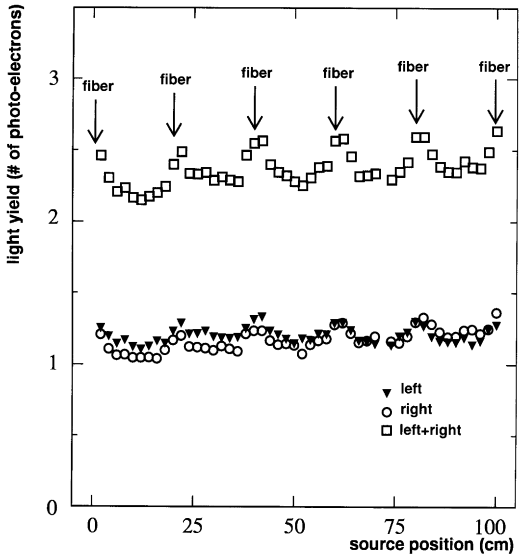

Fig. 3. Light yield vs. position scanned across the WLS fibers (along the vertical arrow (*X*) shown in Fig. 2).

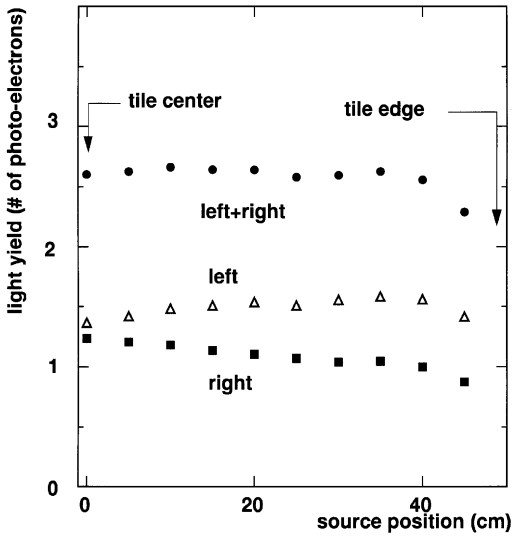

Fig. 4. Light yield vs. position scanned along the fibers from the center to the edge of the tile (along the arrow (*Y*) shown in Fig. 2).

to the fibers (except the points near the fibers) were 5.0 and 2.7%, respectively, while the non-uniformity in a tile in the direction parallel to the fibers was 3%.

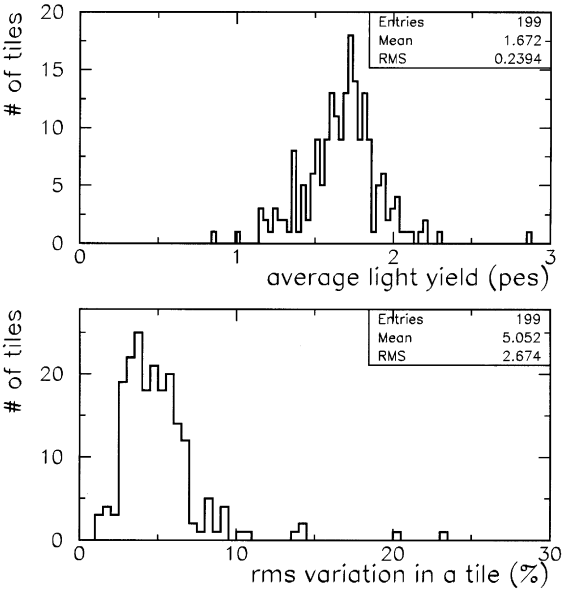

Fig. 5. Distribution of the average light yield (top) and its non-uniformity in a tile (bottom) in the direction across the fibers (except the points near the fibers).

The calorimeter configurations are summarized in Table 1.

3. Experimental setup of the beam test

The beam test was carried out at $\pi 2$ beam line of KEK-PS in two periods, from February to March and from May to June in 1997 which we call T405 and T411, respectively. Experimental setups are shown in Fig. 6.

The measurements were performed with negatively charged particles. The beam energy was set to 1, 2, 3 and 4 GeV. The momentum bite of the beam was 1% (FWHM). The beam was unseparated and contains pions, muons, and electrons. The beam was defined by coincidence of scintillation trigger counters S1, S2, and S3 in T405, and S1, S2, S3, and S4 in T411. The electron trigger required a coincidence between the beam signal and the signals in both Cherenkov counters C1 and C2, filled with CO_2 gas where the pressure of the gas was set to be 1 atm. The muon trigger required a coincidence between the beam signal and the signals

Table 1
Calorimeter configurations tested in T405 and T411. X_0 and λ_I are radiation length and nuclear interaction length, respectively

Configuration in T405 lead : scintillator (in mm)	8 : 2	10 : 2	12 : 2	14 : 2	16 : 2
Number of lead/scintillator layers	105	100	70	70	55
Lead thickness (mm)	8	10	12	14	16
Scintillator thickness (mm)	2	2	2	2	2
Number of superlayers	21	20	14	14	11
Number of PMTs	42	40	28	28	22
Absorber thickness of a superlayer (X_0)	7.14	8.93	10.7	12.5	14.29
Total absorber thickness (λ_I)	4.92	5.85	4.92	5.73	5.15
Total absorber thickness (X_0)	150.0	178.7	150.0	174.7	157.1
Average density of the calorimeter (g/cm^3)	6.64	8.05	7.53	8.35	8.22

Configuration in T411 lead : scintillator (in mm)	4 : 2	6 : 2	8 : 2	10 : 2	16 : 2
Number of lead/scintillator layers	210	160	120	100	55
Lead thickness (mm)	4	6	8	10	16
Scintillator thickness (mm)	2	2	2	2	2
Number of superlayers	42	32	24	20	11
Number of PMTs	84	64	48	40	22
Absorber thickness of a superlayer (X_0)	3.57	5.36	7.14	8.93	14.29
Total absorbe thickness (λ_I)	4.92	5.62	5.62	5.85	5.15
Total absorber thickness (X_0)	150.0	171.1	171.1	178.7	157.1
Average density of the calorimeter (g/cm^3)	6.69	7.41	7.64	8.32	8.81

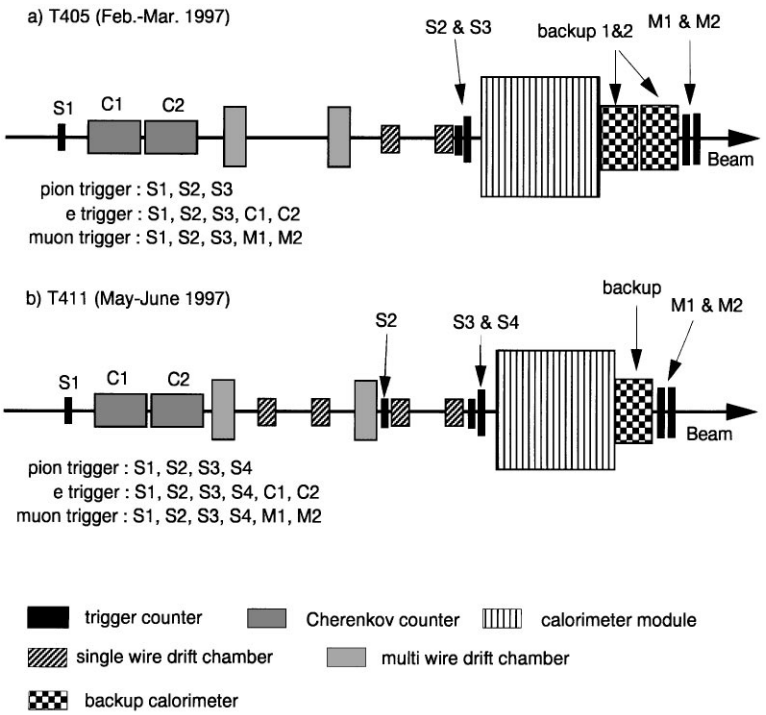

Fig. 6. Schematic layout of the setups of the beam test, (a) for T405 and (b) for T411.

in both muon trigger scintillation counters M1 and M2 located behind the backup calorimeter(s). The pion trigger was just the beam signal, and muons and electrons were reduced in offline analysis.

The fraction of muons in the beam was estimated to be about 1% for the energy of 4 GeV (T405). The fraction of electrons in the beam was estimated to be about 8, 3, 1.5, and 1% for 1, 2, 3, and 4 GeV, respectively (T405).

4. Gain calibration, event selection, and systematic uncertainties

4.1. Gain calibration

The muon events with a beam energy of 4 GeV are used to calibrate the relative gain of the whole readout systems including the phototubes and the ADC since a 4 GeV-muon penetrate through the module as a mip. The absolute energy calibration is done using 4 GeV electron events. The muon trigger data contain a small fraction of pion events. These pions cause an increase in the mean of the pulse height for muon trigger events than that of pure muon events, especially for the forward superlayers. These pions are rejected in offline analysis as described in Section 4.2.

We perform the gain calibration by the following iteration:

(1) Determine initial calibration constants from mean ADC counts for all 4 GeV muon-triggered events.

(2) Select muon events as described in Section 4.2 with gain constants determined by the previous step.

(3) Determine new calibration constants for the selected muon events.

The sequences of (2) and (3) are repeated until calibration constants are converged. Actually two iterations are sufficient. The above gain calibration is performed each time when we altered the calorimeter configuration. Through these procedures, the pion fraction in the muon-triggered data is found to be about 5%. After the muon selection procedure, the fraction of the pions in the muon-selected events become negligible.

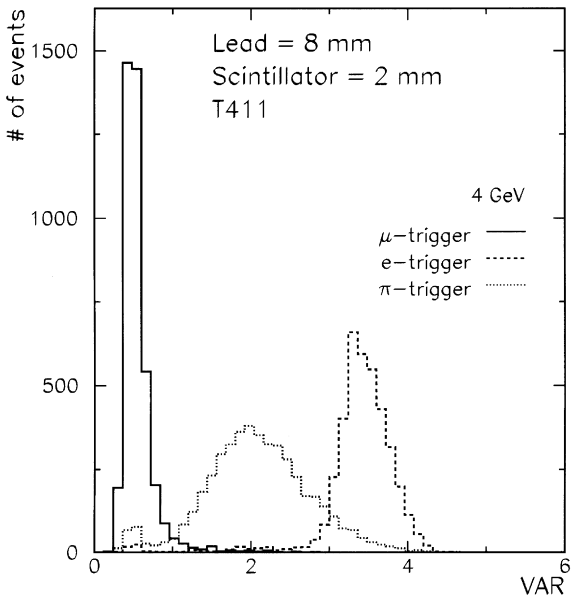

Fig. 7. Typical distribution of the quantity VAR for 4 GeV electron-, μ-, and π-triggered events. The configuration is lead = 8 mm and scintillator = 2 mm.

4.2. Event selection

The selection of the electron, muon, and pion events is based on the longitudinal shower profile measured with the calorimeter itself, in addition to the muon and Cherenkov counters. We defined a quantity VAR as follows:

$$\mathrm{VAR} = \frac{\sqrt{1/(N_{\mathrm{SL}}-1)\sum_{i=1}^{N_{\mathrm{SL}}}(x_i - x_{\mathrm{ave}})^2}}{x_{\mathrm{ave}}},$$

$$x_{\mathrm{ave}} = \frac{1}{N_{\mathrm{SL}}}\sum_{i=1}^{N_{\mathrm{SL}}} x_i \qquad (3)$$

where x_i is the pulse height deposited in ith superlayer, and x_{ave} is the average of pulse heights in a superlayer, and N_{SL} is the number of superlayers.

Shown in Fig. 7 are typical distributions of the quantity VAR for the electron, muon, and pion-triggered events. For muon events, VAR is small because the pulse heights are similar to each other within fluctuations of $\mathrm{d}E/\mathrm{d}x$ and photostatistics. For electron events, pulse heights in forward superlayers are large, and those in backward are zero or

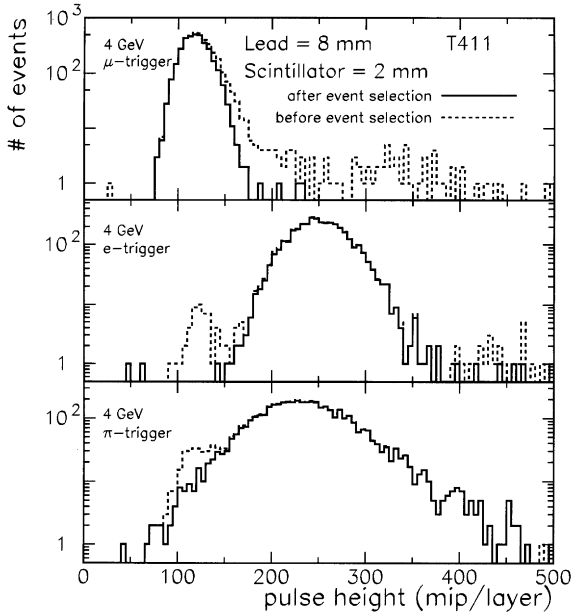

Fig. 8. Typical pulse-height distributions for 4 GeV electrons, muons, and pions before and after event selection. The configuration is lead = 8 mm and scintillator = 2 mm. The dashed histograms are the pulse-height distribution before the event selection. The solid histograms are those after the event selection.

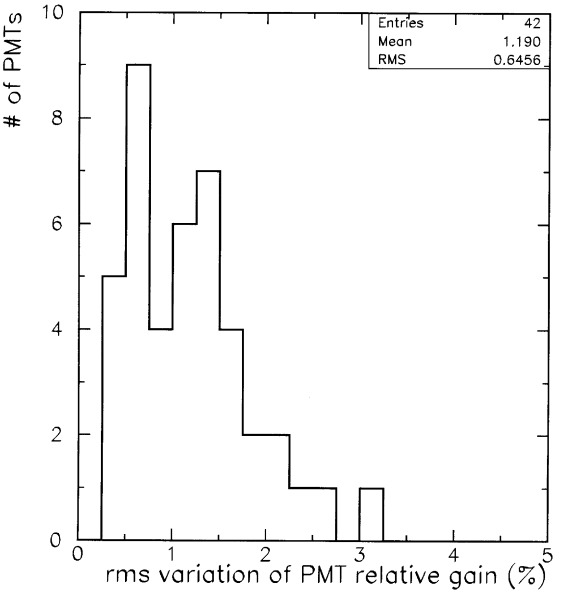

Fig. 9. The distribution of rms variation of relative PMT gain between three muon data sets.

very small. The quantity VAR is thus large for electron events. The VAR for pions distributes between those for muons and electrons. As seen in Fig. 7, there are some muon events in the electron and pion triggers.

The electrons are selected with a cut VAR > 2.5. After this electron selection, the pion contamination in electron triggered events is less than 0.5%. The pions are selected with a cut VAR > 1 and requiring that the both Cherenkov counters have no signals. After this pion selection, contamination by the electrons in the pion events is less than $O(10^{-5})$ and negligibly small to evaluate the performance for pions. The muons are selected with a cut VAR < 1 and requiring that all the superlayers have signals well above the pedestals, and that the pulse height of any superlayer in an event is less than 3.5 mip-equivalent.

Typical pulse height distributions before/after these event selection are shown in Fig. 8, for 4 GeV electrons, muons, and pions for the configuration of 8 mm lead and 2 mm scintillator plates (T411).

4.3. Systematic uncertainties

We have evaluated the following sources of the systematic uncertainties on the energy resolution and the e/π ratio measurements.

(a) PMT gain instability: 1.2% from run to run.

(b) Pedestal instability: Typically 0.75 ADC counts (0.25 pC/count) from run to run, corresponding to a 1.4% change of the gain calibration constants.

(c) Lead thickness variations: 100 μm for a nominal thickness of 4 mm.

(d) Light yield variations of tile/fiber systems: 14% as described in Section 2.

(e) Lateral non-uniformity in a tile/fiber system: 5% as described in Section 2.

Effect of the source (a) is estimated as follows. The change of the gain is obtained using three data sets of penetrating muon runs acquired at different times for the same configuration. The distribution of rms variation of the relative PMT gain between three muon data sets is shown in Fig. 9. The mean

of rms variation of the relative PMT gain is 1.2%. This change of the gain consists of two components; coherent drift of all PMTs, and independent change of each PMT. Energy resolution measurement is affected only by the independent component, while the e/π ratio is affected dominantly by the coherent drift. However, it is not easy to decompose the measured changes into coherent component and independent component. We thus assumed systematic uncertainties conservatively as follows.

- When estimating the effect on energy resolution, we assume that measured gain change is totally incoherent. We randomly change the calibration constants according to the measured shift, and examine the effect on the energy resolution.
- When estimating the effect on the e/π ratio, we assume that measured change is totally coherent. In this case, the e/π ratio simply shifts by an amount of the gain shift. This was taken as the introduced error to the e/π ratio.

We have measured the pedestals frequently, which are used to measure the pedestal instability (b). We examine this effect by comparing the results of the analysis using various pedestal dataset combinations.

Effects of (c), (d), and (e) are estimated using a GEANT 3.2/GHEISHA shower simulation [12]. All the interaction processes available in GEANT are turned on. The cut off energies in the simulation are set to 10 keV for electrons and photons, and 100 keV for the hadrons.

In order to estimate the effect of the source (c), the thicknesses of the lead plates are randomly varied according to the measured precision. Twenty independent configuration sets are made and simulated. The same calibration procedure is applied for these simulated data sets as the case for real data. Examples of performance difference distribution due to lead thickness variation are shown in Fig. 10.

We estimate the effect of the source (d) in the same way as (c). 100 sets of calorimeter configuration are made in which the light yield of each

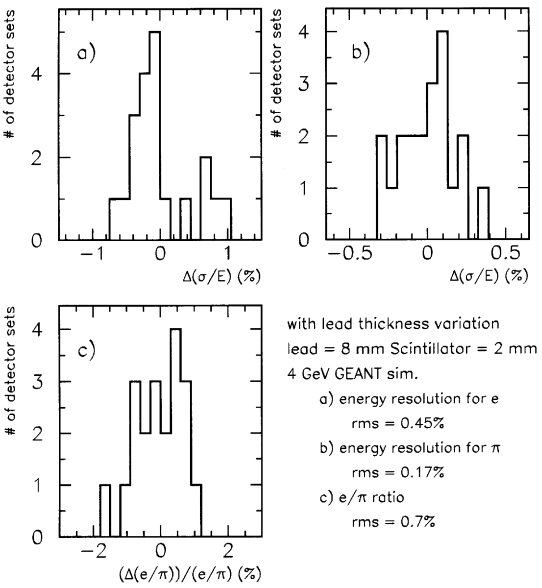

Fig. 10. Typical distributions of performance difference caused by the lead thickness variation; (a) energy resolution for 4 GeV electrons, (b) energy resolution for 4 GeV pions, and (c) e/π ratio for 4 GeV. The configuration is lead = 8 mm and scintillator = 2 mm.

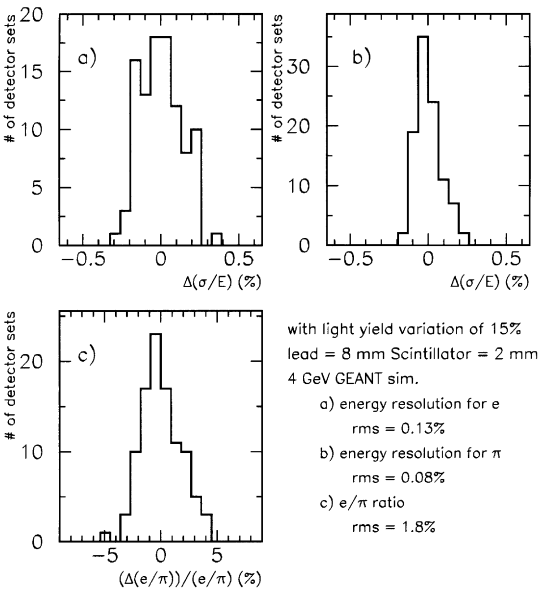

Fig. 11. Typical distributions of performance difference caused by the light yield variation; (a) energy resolution for 4 GeV electrons, (b) energy resolution for 4 GeV pions, and (c) e/π ratio for 4 GeV. The configuration is lead = 8 mm and scintillator = 2 mm.

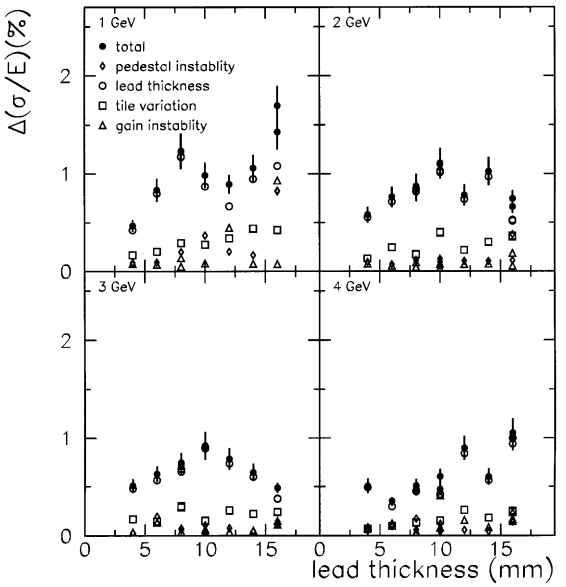

Fig. 12. Systematic uncertainty on energy resolution for electrons.

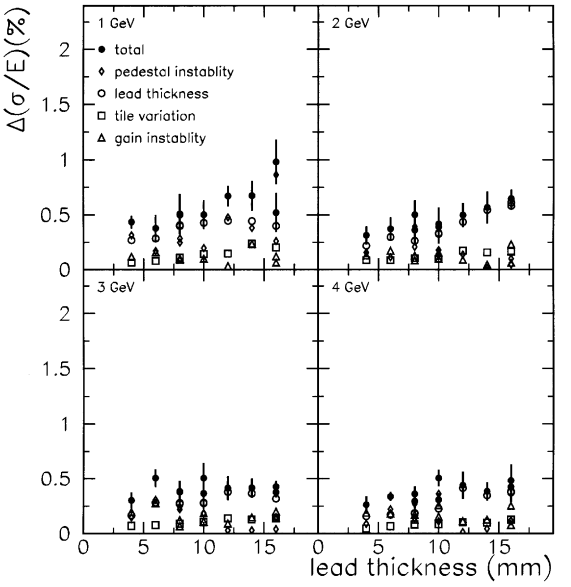

Fig. 13. Systematic uncertainty on energy resolution for pions.

tile/fiber system is smeared according to a Gaussian distribution with a standard deviation of 15%. Examples of such distributions are shown in Fig. 11.

Effect of the source (e) is examined similarly. A scintillator tile is divided into 100 strips of 1 cm wide, and each response is varied according to the measured response map. Average light yield is kept same for all the tile/fiber systems, since the light yield variation in different tile/fiber systems is taken into account in (d).

Systematic uncertainties obtained in the above on the energy resolution and e/π ratio are plotted in Figs. 12–14. Typical total systematic uncertainties are 0.5, 0.3, and 2.3% on the energy resolution σ/E for 4 GeV electrons, σ/E for 4 GeV pions, and the e/π ratio for 4 GeV, respectively, for the configuration of 8 mm lead and 2 mm scintillator plates (T411). We note that the lead thickness variation is the dominant source for the systematic uncertainty on the energy resolution (Figs. 12 and 13), while the tile gain variation is dominant on the e/π ratio (Fig. 14). The change in the performance due to (e) is negligible, and therefore is not plotted. Error

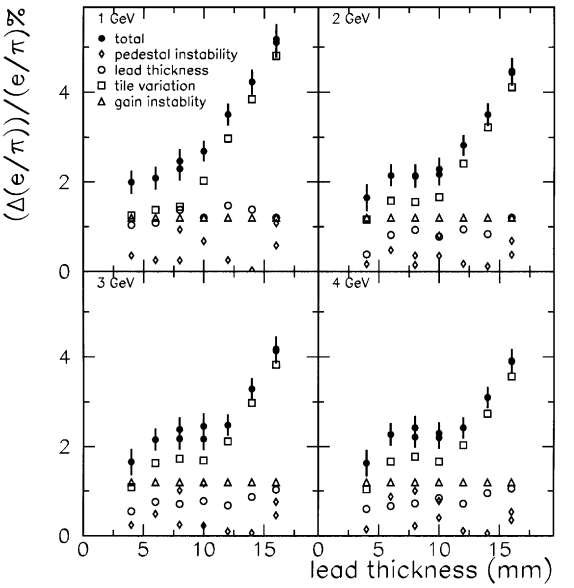

Fig. 14. Systematic uncertainty on e/π ratio.

bars shown in the figures are the statistical errors in estimating the total systematic uncertainty. Total systematic uncertainties are summarized in Table 2.

Table 2
Total systematic uncertainties on energy resolution for electrons (top), for pions (middle), and the e/π ratio (bottom)

Configuration lead : scintillator (in mm)	$\Delta(\sigma/E)$ for electrons (%)			
	1 GeV	2 GeV	3 GeV	4 GeV
4 : 2 in T411	0.5	0.6	0.5	0.5
6 : 2 in T411	0.8	0.8	0.6	0.4
8 : 2 in T405	1.2	0.8	0.7	0.5
8 : 2 in T411	1.2	0.8	0.7	0.5
10 : 2 in T405	1.0	1.1	0.9	0.5
10 : 2 in T411	No data	1.1	0.9	0.6
12 : 2 in T405	0.9	0.8	0.8	0.9
14 : 2 in T405	1.1	1.0	0.6	0.6
16 : 2 in T405	1.7	0.8	0.5	1.0
16 : 2 in T411	1.4	0.7	0.5	1.1

Configuration lead : scintillator (in mm)	$\Delta(\sigma/E)$ for pions (%)			
	1 GeV	2 GeV	3 GeV	4 GeV
4 : 2 in T411	0.4	0.3	0.3	0.3
6 : 2 in T411	0.4	0.4	0.5	0.3
8 : 2 in T405	0.5	0.5	0.4	0.4
8 : 2 in T411	0.5	0.4	0.4	0.3
10 : 2 in T405	0.5	0.5	0.4	0.3
10 : 2 in T411	No data	0.5	0.5	0.5
12 : 2 in T405	0.7	0.5	0.4	0.4
14 : 2 in T405	0.7	0.6	0.4	0.4
16 : 2 in T405	1.0	0.6	0.4	0.4
16 : 2 in T411	0.5	0.6	0.4	0.5

Configuration lead : scintillator (in mm)	$(\Delta(e/\pi))/(e/\pi)$ (%)			
	1 GeV	2 GeV	3 GeV	4 GeV
4 : 2 in T411	2.1	1.7	1.7	1.7
6 : 2 in T411	2.1	2.2	2.2	2.3
8 : 2 in T405	2.5	2.2	2.4	2.5
8 : 2 in T411	2.3	2.2	2.2	2.3
10 : 2 in T405	2.7	2.2	2.2	2.2
10 : 2 in T411	No data	2.3	2.5	2.5
12 : 2 in T405	3.5	2.9	2.5	2.5
14 : 2 in T405	4.3	3.5	3.3	3.1
16 : 2 in T405	5.2	4.5	4.2	3.9
16 : 2 in T411	5.1	4.5	4.2	3.9

5. The results

5.1. Energy resolution for electrons

Energy resolution for electrons is obtained by fitting pulse-height distributions with a single Gaussian function over the region $\pm 2.5\sigma$ around the mean. The measured energy resolution σ/E for electrons is listed in Table 3.

Energy resolution is well described by the following equation:

$$\frac{\sigma}{E} = \frac{\sigma_{\text{stochastic}}}{\sqrt{E}} \oplus \sigma_{\text{constant}} \tag{4}$$

where $\oplus$ denotes the sum in quadrature and E is energy in GeV. In general, the sources of σ_{constant} are calibration uncertainty, shower leakage and non-uniformity of the calorimeter. A fitting with Eq. (4) to the measured energy resolution σ/E is performed, and the results of the fitting are listed in Table 4. As shown in Table 4, the constant terms are consistent to zero in most cases, but errors are large. Thus they are disregarded in following analyses. This is reasonable in such a low energy range we measured.

The stochastic term for a sampling calorimeter is given by

$$\sigma_{\text{stochastic}}/\sqrt{E} = \sqrt{\sigma^2_{\text{intrinsic}} + (\sigma^2_{\text{sample}} + \sigma^2_{\text{photostat}}) \times d}/\sqrt{E} \tag{5}$$

where d is the thickness of a lead plate in mm, $\sigma_{\text{intrinsic}}$ depends on the interaction of the secondary particles, σ_{sample} is the sampling fluctuation, and $\sigma_{\text{photostat}}$ comes from the statistical fluctuation of the number of photo-electrons.

Energy dependence and lead-thickness dependence of the energy resolution $\sigma/\sqrt{E}$ for each calorimeter configuration are shown in Figs. 15 and 16, respectively. We can see in Fig. 15 that $\sigma_{\text{stochastic}}$ is dominant in the energy resolution for electrons as described above. Since $\sigma/\sqrt{E}$ is dominated by $\sigma_{\text{stochastic}}$, we can fit the data in Fig. 16 with Eq. (5).

The fitted result is

$$\sigma_{\text{intrinsic}} = 0.0^{+1.3}_{-0.0}\% \text{ and}$$

$$\sqrt{\sigma^2_{\text{sample}} + \sigma^2_{\text{photostat}}} = (8.31 \pm 0.06)\%$$

with $\chi^2/\text{n.d.f.} = 43.7/37 = 1.18$.

The photostatistic term was estimated to be $(3.8 \pm 0.1)\%$ from the light yield measurement of tile/fiber systems described in Section 2. Thus, σ_{sample} was estimated to be $(7.4 \pm 0.1)\%$. For EM shower, $\sigma_{\text{intrinsic}}$ is negligible.

Table 3
The energy resolution σ/E for electrons

Configuration lead : scintillator (in mm)	σ/E (%)			
	1 GeV	2 GeV	3 GeV	4 GeV
4 : 2 in T411	15.1 ± 0.5	11.0 ± 0.6	8.7 ± 0.5	7.6 ± 0.5
6 : 2 in T411	19.3 ± 0.9	14.5 ± 0.8	11.1 ± 0.7	9.8 ± 0.4
8 : 2 in T405	22.9 ± 1.3	16.6 ± 0.9	13.6 ± 0.8	11.6 ± 0.5
8 : 2 in T411	22.9 ± 1.3	16.2 ± 0.9	13.2 ± 0.7	11.2 ± 0.5
10 : 2 in T405	25.3 ± 1.0	18.6 ± 1.1	15.3 ± 0.9	13.3 ± 0.5
10 : 2 in T411	No data	18.8 ± 1.1	15.5 ± 0.9	13.1 ± 0.6
12 : 2 in T405	27.1 ± 1.0	20.9 ± 0.8	17.1 ± 0.8	14.8 ± 0.9
14 : 2 in T405	31.0 ± 1.2	23.0 ± 1.1	18.8 ± 0.7	16.5 ± 0.7
16 : 2 in T405	34.1 ± 1.7	25.1 ± 0.8	20.3 ± 0.5	16.9 ± 1.0
16 : 2 in T411	33.2 ± 1.6	24.5 ± 0.8	20.0 ± 0.6	18.1 ± 1.1

Table 4
The σ/E fit result with Eq. (4) for electrons

Calorimeter configuration	$\sigma_{\text{stochastic}}$ (%)	σ_{constant} (%)
Lead : scintillator = 4 : 2 mm in T411	15.2 ± 0.6	$0.0^{+3.4}_{-0.0}$
Lead : scintillator = 6 : 2 mm in T411	19.5 ± 0.9	$1.3^{+4.1}_{-1.3}$
Lead : scintillator = 8 : 2 mm in T405	23.0 ± 1.2	$1.9^{+5.3}_{-1.9}$
Lead : scintillator = 8 : 2 mm in T411	22.7 ± 0.9	$0.0^{+4.2}_{-0.0}$
Lead : scintillator = 10 : 2 mm in T405	25.0 ± 1.4	$4.6^{+6.8}_{-4.6}$
Lead : scintillator = 10 : 2 mm in T411	26.5 ± 1.9	$0.0^{+6.6}_{-0.0}$
Lead : scintillator = 12 : 2 mm in T405	26.5 ± 1.5	7.6 ± 2.4
Lead : scintillator = 14 : 2 mm in T405	30.5 ± 1.5	6.6 ± 3.0
Lead : scintillator = 16 : 2 mm in T405	35.0 ± 1.3	$0.0^{+7.1}_{-0.0}$
Lead : scintillator = 14 : 2 mm in T405	32.9 ± 2.0	$6.8^{+9.9}_{-6.8}$

5.2. Energy resolution for pions

Energy resolution for pions is obtained with the same procedure as for electrons. The measured energy resolution σ/E for pions is listed in Table 5.

A fitting with Eq. (4) to the measured energy resolution σ/E is performed, for 2, 3, and 4 GeV, and the results of the fitting are listed in Table 6. As shown in Table 6, the constant terms are again consistent to zero in most cases, but could not be estimated precisely and were disregarded, same as electrons.

The best energy resolution for pions of $33.6\%/\sqrt{E}$ is obtained with the configuration where the thicknesses of lead and scintillator plate were 4 and 2 mm, respectively.

The results for each energy and each configuration are shown in Figs. 17 and 18. As seen in Fig. 17, $\sigma_{\text{stochastic}}$ is also dominant for pions in the energy range we measured as described above. Thus $\sigma/\sqrt{E}$ was fitted with Eq. (5) as a function of lead thickness as shown in Fig. 18. Here the data for 2, 3, and 4 GeV and those for 1 GeV are fitted separately, since 1 GeV shower behaves differently as seen in Fig. 17.

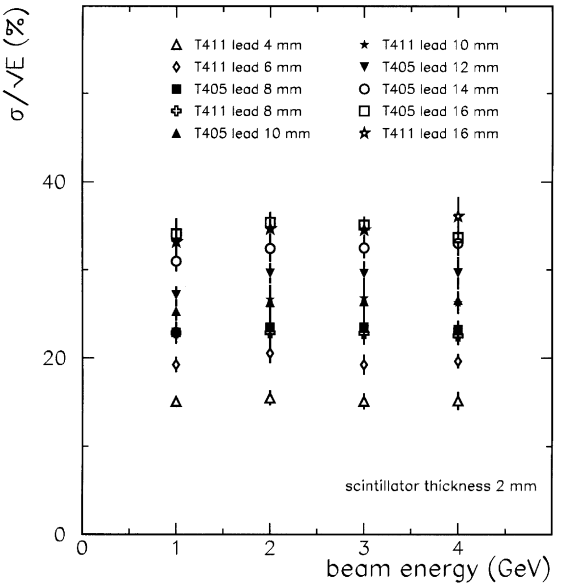

Fig. 15. Energy resolution $\sigma/\sqrt{E}$ vs. energy for electrons.

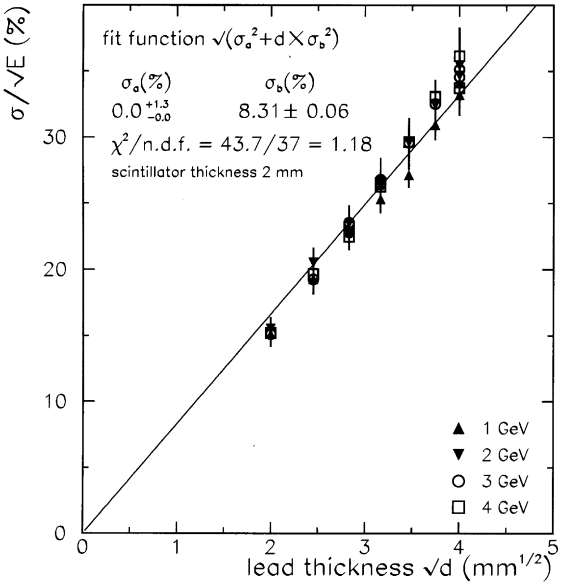

Fig. 16. Energy resolution $\sigma/\sqrt{E}$ vs. Pb thickness for electrons. Solid curve is a fit to Eq. (5).

The results are

$\sigma_{\text{intrinsic}} = (24.4 \pm 0.7)\%$

and

$\sqrt{\sigma^2_{\text{sample}} + \sigma^2_{\text{photostat}}} = (11.2 \pm 0.2)\%$

for 2, 3, and 4 GeV

$\sigma_{\text{intrinsic}} = (25.6 \pm 0.9)\%$

and

$\sqrt{\sigma^2_{\text{sample}} + \sigma^2_{\text{photostat}}} = (8.9 \pm 0.3)\%$ for 1 GeV.

χ^2/n.d.f. of these fittings are $24.0/28 = 0.86$ (for 2, 3, 4 GeV) and $3.32/7 = 0.474$ (for 1 GeV). $\sigma_{\text{intrinsic}}$ is estimated to be about 25% for lead/scintillator sampling calorimeters. As $\sigma_{\text{photostat}}$ is estimated to be $(3.8 \pm 0.1)\%$, σ_{sample} are estimated to be

Table 5
The energy resolution σ/E for pions

Configuration lead : scintillator (in mm)	σ/E (%)			
	1 GeV	2 GeV	3 GeV	4 GeV
4 : 2 in T411	31.4 ± 0.6	24.4 ± 0.5	19.1 ± 0.4	16.5 ± 0.4
6 : 2 in T411	33.7 ± 0.6	25.7 ± 0.5	21.1 ± 0.6	17.3 ± 0.5
8 : 2 in T405	35.7 ± 0.6	28.1 ± 0.6	22.6 ± 0.4	20.0 ± 0.5
8 : 2 in T411	35.7 ± 0.7	28.0 ± 0.6	23.3 ± 0.5	19.7 ± 0.4
10 : 2 in T405	38.3 ± 0.8	30.3 ± 0.6	24.9 ± 0.5	21.5 ± 0.4
10 : 2 in T411	No data	30.8 ± 0.7	25.3 ± 0.7	21.7 ± 0.6
12 : 2 in T405	40.6 ± 1.0	32.6 ± 0.7	26.8 ± 0.6	23.2 ± 0.6
14 : 2 in T405	40.6 ± 1.0	32.9 ± 0.8	27.3 ± 0.6	24.5 ± 0.5
16 : 2 in T405	44.6 ± 1.3	36.0 ± 0.9	29.8 ± 0.6	26.6 ± 0.6
16 : 2 in T411	44.7 ± 1.1	34.9 ± 1.0	29.9 ± 0.6	26.1 ± 0.7

Table 6
The σ/E fit result with Eq. (4) for pions

Calorimeter configuration	$\sigma_{\text{stochastic}}$ (%)	σ_{constant} (%)
Lead : scintillator = 4 : 2 mm in T411	33.6 ± 0.5	$0.0^{+3.1}_{-0.0}$
Lead : scintillator = 6 : 2 mm in T411	36.0 ± 0.6	$0.0^{+4.0}_{-0.0}$
Lead : scintillator = 8 : 2 mm in T405	39.4 ± 1.3	$1.9^{+7.3}_{-1.9}$
Lead : scintillator = 8 : 2 mm in T411	39.7 ± 1.0	$0.0^{+6.2}_{-0.0}$
Lead : scintillator = 10 : 2 mm in T405	42.7 ± 0.5	$2.6^{+7.7}_{-2.6}$
Lead : scintillator = 10 : 2 mm in T411	43.6 ± 1.4	$0.0^{+8.0}_{-0.0}$
Lead : scintillator = 12 : 2 mm in T405	45.8 ± 1.7	$3.9^{+9.2}_{-3.9}$
Lead : scintillator = 14 : 2 mm in T405	43.6 ± 2.5	11.9 ± 3.3
Lead : scintillator = 16 : 2 mm in T405	48.3 ± 2.8	11.0 ± 4.4
Lead : scintillator = 14 : 2 mm in T405	46.8 ± 3.2	12.0 ± 4.4

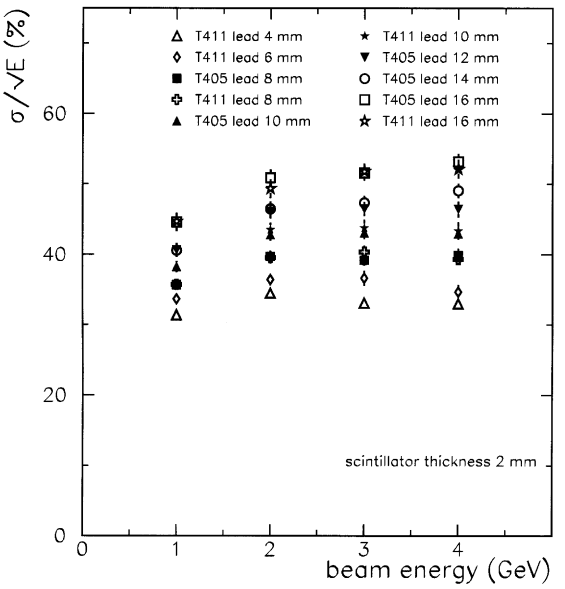

Fig. 17. Energy resolution $\sigma/\sqrt{E}$ vs. energy for pions.

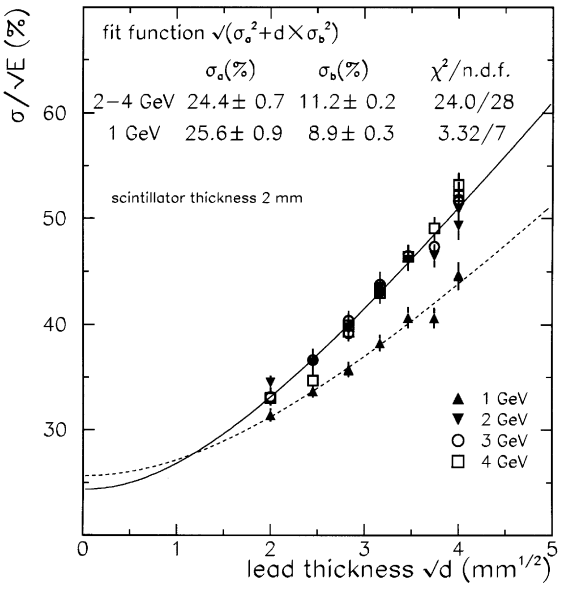

Fig. 18. Energy resolution $\sigma/\sqrt{E}$ vs. Pb thickness for pions. Solid and dashed curves shown in the figure are fitting results to Eq. (5) for 2–4 and 1 GeV, respectively.

$(10.5 \pm 0.2)\%$ for 2–4 GeV and $(8.0 \pm 0.3)\%$ for 1 GeV.

As shown in Fig. 18, $\sigma_{\text{stochastic}}$ for 1 GeV pions is smaller than those for 2–4 GeV, indicating that 1 GeV pions do not develop shower sufficiently.

5.3. *Linearity, the e/π pulse-height ratio, and, lateral leak correction*

In order to calculate linearity and the e/π pulse-height ratio, shower leakage must be corrected for

Table 7
The non-linearity

Calorimeter configuration	For electrons (%)	For pions (%)
Lead : scintillator = 4 : 2 mm in T411	1.2 ± 0.4	1.0 ± 0.3
Lead : scintillator = 6 : 2 mm in T411	1.1 ± 0.4	1.2 ± 0.4
Lead : scintillator = 8 : 2 mm in T405	2.2 ± 0.7	1.1 ± 0.5
Lead : scintillator = 8 : 2 mm in T411	2.7 ± 1.0	1.0 ± 0.3
Lead : scintillator = 10 : 2 mm in T405	2.7 ± 1.0	0.9 ± 0.4
Lead : scintillator = 10 : 2 mm in T411	1.1 ± 0.5	1.1 ± 0.5
Lead : scintillator = 12 : 2 mm in T405	2.7 ± 1.0	2.1 ± 0.8
Lead : scintillator = 14 : 2 mm in T405	2.8 ± 1.0	2.4 ± 1.0
Lead : scintillator = 16 : 2 mm in T405	3.4 ± 1.2	3.7 ± 1.3
Lead : scintillator = 16 : 2 mm in T405	1.6 ± 0.6	3.3 ± 1.3

Table 8
The lateral shower leakage estimated from the lateral shower profile function measured by SPACAL experiment [13]

Configuration lead : scintillator (in mm)	Lateral leakage (%)			
	1 GeV	2 GeV	3 GeV	4 GeV
4 : 2 in T411	5.8 ± 1.7	5.3 ± 1.6	5.0 ± 1.5	4.7 ± 1.4
6 : 2 in T411	4.5 ± 1.4	4.1 ± 1.2	3.9 ± 1.2	3.7 ± 1.1
8 : 2 in T405	5.9 ± 1.8	5.4 ± 1.6	5.1 ± 1.5	4.8 ± 1.5
8 : 2 in T411	4.1 ± 1.2	3.8 ± 1.1	3.6 ± 1.1	3.4 ± 1.0
10 : 2 in T405	3.5 ± 1.1	3.2 ± 1.0	3.1 ± 0.9	2.9 ± 0.9
10 : 2 in T411	—	3.0 ± 0.9	2.9 ± 0.9	2.8 ± 0.9
12 : 2 in T405	4.1 ± 1.2	3.8 ± 1.1	3.6 ± 1.1	3.4 ± 1.0
14 : 2 in T405	3.1 ± 0.9	2.9 ± 0.9	2.7 ± 0.8	2.6 ± 0.8
16 : 2 in T405	3.4 ± 1.0	3.1 ± 0.9	2.9 ± 0.9	2.8 ± 0.8
16 : 2 in T411	2.8 ± 0.8	2.5 ± 0.8	2.4 ± 0.7	2.3 ± 0.7

the pion shower. This correction is done by using parameterized shower profile obtained by SPACAL experiment [13] as

$$\frac{dE}{ds} = \frac{B_1}{r}\exp\left(-\frac{r}{\lambda_1}\right) + \frac{B_2}{r}\exp\left(-\frac{r^2}{\lambda_2^2}\right). \quad (6)$$

However, SPACAL data exist only for configuration of lead/scintillator $= \frac{8}{2}$ and for energies higher than or equal to 5 GeV. We thus extrapolate the shower profile parameters according to the average calorimeter density and energy dependence of the leakage fraction.

Energy dependence of the lateral leak is estimated by simply extrapolating the energy dependence of the lateral leak fraction measured by SPACAL experiment (Fig. 18 of Ref. [13]). Our estimation from the extrapolation is given below.

leak at 1 GeV = leak at 5 GeV × 1.25,

leak at 2 GeV = leak at 5 GeV × 1.15,

leak at 3 GeV = leak at 5 GeV × 1.09, and

leak at 4 GeV = leak at 5 GeV × 1.03.

Here relative error for shower leak at 5 GeV is estimated to be ± 30% in Ref. [13].

Density dependence is calculated by scaling the lateral size parameters λ_1 and λ_2 inversely proportional to the average density of the calorimeter. For

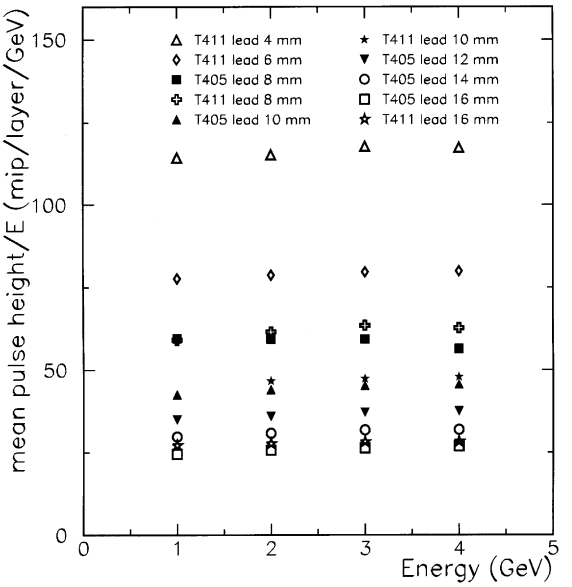

Fig. 19. Mean pulse height/energy vs. energy for electrons.

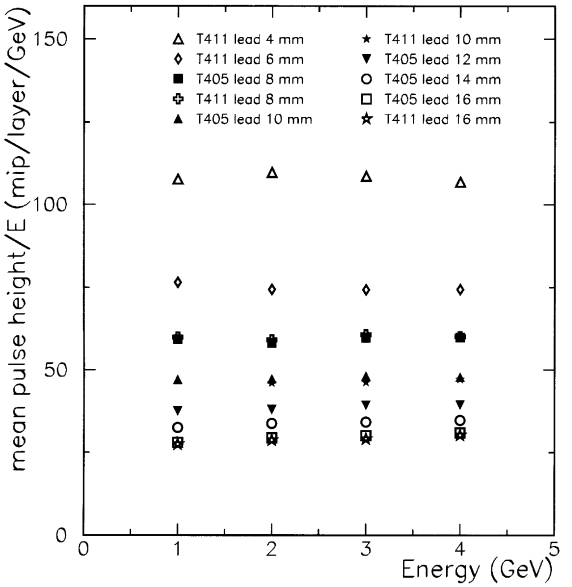

Fig. 20. Mean pulse height/energy vs. energy for pions.

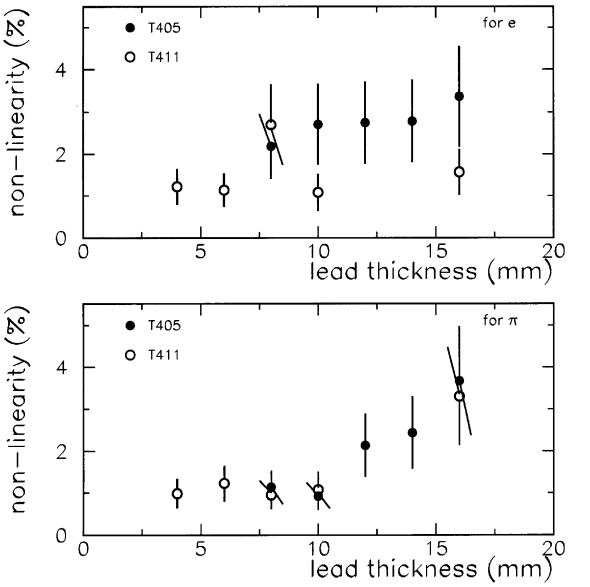

Fig. 21. Non-linearity vs. lead thickness for electrons (top) and for pions (above).

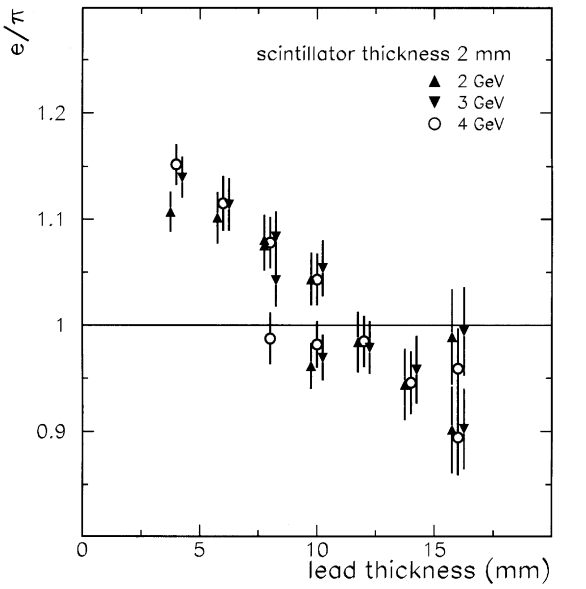

Fig. 22. The e/π ratio (uncorrected) vs. Pb thickness. The error is dominated by systematic uncertainties introduced when the lead thickness is changed. Therefore, the errors are correlated for the data in the same configuration, thus irreducible by combining data of same configuration.

example, in the case of 8 : 2 configuration of T411 beam test, the average density of the calorimeter module was 6.69 g/cm^3 (Table 7). SPACAL group obtained lateral size parameter $\lambda_1 = 17.7$ cm and

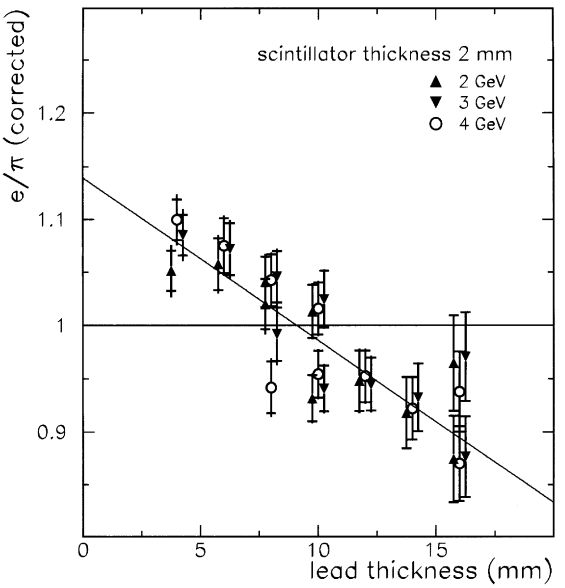

Fig. 23. The e/π ratio (corrected) vs. Pb thickness. The error is dominated by systematic uncertainties introduced when the lead thickness is changed. The inner error bar in the plot shows the statistical and systematic uncertainty without lateral leakage correction. The outer error in the plot shows the total uncertainty including lateral leakage correction. The line in the plot is the result of linear function fitting to data. We obtained the compensation point to be $d = 9.1 \pm 0.3$ mm from this fitting.

$\lambda_2 = 7.68$ cm for their module which had an average density of 9.02 g/cm^3. Assuming these size parameters are inversely proportional to the calorimeter density, we obtain $\lambda_1 = 23.9$ cm and $\lambda_2 = 10.4$ cm for our 8 : 2 module. Using these parameters, shower profile function (6) is numerically integrated over 1 m^2 and over infinitely, and leak fraction is obtained. The results of these lateral shower leakage are listed in Table 8.

The mean of the pulse-height distribution is obtained by fitting with a Gaussian. Figs. 19 and 20 show the mean pulse height divided by the beam energy. We can see in these figures that pulse height is described by a linear function of the energy. Non-linearity is defined by the rms variation of the mean pulse height/energy for each configuration, and is shown in Fig. 21. The linearity is degraded for thick lead absorbers due to coarse sampling. Otherwise linearity is reasonable.

The e/π ratio before and after lateral leakage correction are plotted in Figs. 22 and 23 as a function of the absorber thickness, and also listed in Tables 9 and 10 . The 1 GeV data is omitted from Figs. 22 and 23 since 1 GeV pion shower behaves differently as seen in Fig. 18. As seen from Fig. 23, the e/π ratio decreases as the lead thickness increases, and crosses the line of $e/\pi = 1$. Since $e/\pi = 1$ equivalently means $e/h = 1$, this point gives the compensation condition. This behaviour is approximated by a linear function and fitting is carried out. The result of the fitting is also shown in Fig. 23. As a result of this fitting, the compensation point is found to be 9.1 ± 0.3 mm for 2 mm-thick plastic scintillator. This fitted e/π ratio is significantly smaller than the previous measurements

Table 9
The e/π ratio (before lateral leakage correction)

Configuration lead : scintillator (in mm)	e/π			
	1 GeV	2 GeV	3 GeV	4 GeV
4 : 2 in T411	1.12 ± 0.02	1.11 ± 0.02	1.14 ± 0.02	1.15 ± 0.02
6 : 2 in T411	1.06 ± 0.02	1.10 ± 0.02	1.11 ± 0.03	1.11 ± 0.03
8 : 2 in T405	1.06 ± 0.03	1.08 ± 0.02	1.04 ± 0.03	0.99 ± 0.03
8 : 2 in T411	1.03 ± 0.02	1.08 ± 0.02	1.08 ± 0.02	1.08 ± 0.02
10 : 2 in T405	0.94 ± 0.03	0.96 ± 0.02	0.97 ± 0.02	0.98 ± 0.02
10 : 2 in T411	No data	1.04 ± 0.03	1.05 ± 0.03	1.04 ± 0.03
12 : 2 in T405	0.97 ± 0.04	0.98 ± 0.03	0.98 ± 0.03	0.98 ± 0.02
14 : 2 in T405	0.95 ± 0.04	0.94 ± 0.03	0.96 ± 0.03	0.95 ± 0.03
16 : 2 in T405	0.91 ± 0.05	0.90 ± 0.04	0.90 ± 0.04	0.89 ± 0.04
16 : 2 in T411	1.02 ± 0.05	0.99 ± 0.05	0.99 ± 0.04	0.96 ± 0.04

Table 10
The e/π ratio (after lateral leakage correction)

Configuration lead : scintillator (in mm)	e/π			
	1 GeV	2 GeV	3 GeV	4 GeV
4 : 2 in T411	1.06 ± 0.03	1.05 ± 0.03	1.09 ± 0.03	1.10 ± 0.02
6 : 2 in T411	1.01 ± 0.03	1.06 ± 0.03	1.07 ± 0.03	1.08 ± 0.03
8 : 2 in T405	1.00 ± 0.03	1.02 ± 0.03	0.99 ± 0.03	0.94 ± 0.03
8 : 2 in T411	0.99 ± 0.03	1.04 ± 0.03	1.05 ± 0.03	1.04 ± 0.03
10 : 2 in T405	0.91 ± 0.03	0.93 ± 0.02	0.94 ± 0.02	0.95 ± 0.02
10 : 2 in T411	No data	1.01 ± 0.03	1.02 ± 0.03	1.02 ± 0.03
12 : 2 in T405	0.93 ± 0.04	0.95 ± 0.03	0.94 ± 0.03	0.95 ± 0.03
14 : 2 in T405	0.92 ± 0.04	0.92 ± 0.03	0.93 ± 0.03	0.92 ± 0.03
16 : 2 in T405	0.88 ± 0.05	0.87 ± 0.04	0.88 ± 0.04	0.87 ± 0.04
16 : 2 in T411	0.99 ± 0.05	0.96 ± 0.05	0.97 ± 0.04	0.94 ± 0.04

[4–6] which gave $e/\pi = 1.1$ for $E \leq 10$ GeV with configuration of 8 : 2.

6. Conclusions

We measure the energy resolution and the e/π ratio of lead/plastic-scintillator sampling calorimeter for various lead/scintillator volume ratios in the energy range 1–4 GeV.

The energy resolution for electrons is measured to be $\sigma/E = (0.0^{+1.3}_{-0.0}\% \oplus (8.30 \pm 0.06\%) \times \sqrt{\mathrm{d}})/\sqrt{E}$, where the thickness d of lead plate is in mm and the energy E is in GeV. Energy resolution for pions is measured to be $\sigma/E = (24.4 \pm 0.7\% \oplus (11.2 \pm 0.2\%) \times \sqrt{d}/\sqrt{E}$ for 2–4 GeV and $\sigma/E = (25.6 \pm 0.9\% \oplus (8.9 \pm 0.3\%) \times \sqrt{d}/\sqrt{E}$ for 1 GeV.

The best hadron energy resolution of $33.6\%/\sqrt{E}$ is obtained for 4 mm thick lead absorber case. This is as good as typical lead/scintillating-fiber calorimeter, and is one of the best energy resolutions achieved so far. This enables us to construct a linear collider calorimeter with the best hadron energy resolution at a reasonable cost. The intrinsic hadron energy resolution of $25\%\sqrt{E}$ would suggest us to design an ambitious calorimeter with a much better resolution.

The compensation is found to be achieved at the lead thickness of 9.1 ± 0.3 mm in combination with 2 mm-thick plastic scintillator. This ratio is a little larger than those popularly assumed. However, tests with higher-energy beams are necessary to confirm the consistency with the existing data.

Acknowledgements

We would like to thank the members of the accelerator group and the beam channel group of the KEK proton synchrotron for their support during the beam test. This work was supported in part by KEK-University R&D program and by the JSPS Japanese–German Cooperative Program.

References

[1] JLC Group, KEK Report, vol. 92–16, 1992.
[2] R. Wigman, Nucl. Instr. and Meth. A 259 (1987) 389.
[3] R. Wigmans, Proceedings of the second International Conference on Calorimetry in High Energy Physics, Capri, Italy, 1991, CERN-PPE, vol. 91–205, 1991.
[4] E. Bernardi et al., Nucl. Instr. and Meth. A 262 (1987) 229.
[5] D. Acosta et al., Nucl. Instr. and Meth. A 308 (1991) 481.
[6] K. Ishii et al., Nucl. Instr. and Meth. A 385 (1997) 215.
[7] The CDF II Collaboration, The CDF II Detector Technical Design Report FELMILAB-Pub-96/390-E, 1996.

[8] T. Asakawa et al., Nucl. Instr. and Meth. A 340 (1994) 458. S. Aota et al., Nucl. Instr. and Meth. A 352 (1995) 557.
[9] S. Kim (CDF Collaboration), Nucl. Instr. and Meth. A 360 (1995) 206.
[10] S. Aota et al., Nucl. Instr. and Meth. A 357 (1995) 71.
[11] K. Hara et al., Nucl. Instr. and Meth. A 348 (1994) 139.
[12] R. Brun et al., "GEANT3" CERN DD/EE/84-1.
[13] D. Acosta et al., Nucl. Instr. and Meth. A 316 (1992) 184.